RNAi screening identifies the armadillo repeat-containing kinesins responsible for microtubule-dependent nuclear positioning in *Physcomitrella patens*

Tomohiro Miki[1,2], Momoko Nishina[1], and Gohta Goshima[1,2†]

[1]Division of Biological Science, Graduate School of Science, Nagoya University, Furo-cho, Chikusa-ku, Nagoya 464-8602, Japan
[2]Marine Biological Laboratory, Woods Hole, MA02543, USA

[†]To whom correspondence should be addressed.
E-mail: goshima@bio.nagoya-u.ac.jp
Phone: +81 52-788-6175; Fax: +81 52-788-6174

Running title: The functions of kinesin-ARK in *P. patens*

Key words: Kinesin, nuclear positioning, microtubule, RNAi screening, *Physcomitrella patens*

List of abbreviations: armadillo repeat-containing kinesin (kinesin-ARK), double-stranded RNA (dsRNA), microtubule (MT), *N*-ethylmaleimide (NEM), nuclear envelope (NE), quantitative real-time reverse transcription PCR (qRT-PCR), RNA interference (RNAi), total internal reflection fluorescence microscope (TIRFM).

Abstract

Proper positioning of the nucleus is critical for the functioning of various cells. Actin and myosin have been shown to be crucial for the localisation of the nucleus in plant cells, whereas microtubule (MT)-based mechanisms are commonly utilised in animal and fungal cells. In this study, we combined live cell microscopy with RNA interference (RNAi) screening or drug treatment and showed that MTs and a plant-specific motor protein, armadillo repeat-containing kinesin (kinesin-ARK), are required for nuclear positioning in the moss *Physcomitrella patens*. In tip-growing protonemal apical cells, the nucleus was translocated to the centre of the cell after cell division in an MT-dependent manner. When kinesin-ARKs were knocked down using RNAi, the initial movement of the nucleus towards the centre took place normally; however, before reaching the centre, the nucleus was moved back to the basal edge of the cell. In intact (control) cells, MT bundles that are associated with kinesin-ARKs were frequently observed around the moving nucleus. In contrast, such MT bundles were not identified after kinesin-ARK downregulation. An *in vitro* MT-gliding assay showed that kinesin-ARK is a plus-end-directed motor protein. These results indicate that MTs and the MT-based motor drive nuclear migration in the moss cells, thus showing a conservation of the mechanism underlying nuclear localisation among plant, animal, and fungal cells.

Introduction

Eukaryotic cells have a nucleus that envelops genetic material along with regulators of gene expression. In many cell types, the nucleus is not randomly positioned in a cell (Gundersen and Worman 2013). For example, cells of rod-shaped fission yeast keep the nucleus at the centre of the cell, and consequently form the mitotic spindle and the cytokinetic contractile ring at the cell centre; these mechanisms ensure symmetrical cell division (Tran et al. 2001). In contrast, in many types of differentiated animal cells such as epithelial cells and neurons, the nucleus is positioned asymmetrically, which might be necessary for the cell's physiology (Gundersen and Worman 2013). Such altered positioning of the nucleus is also observed in plant cells, sometimes brought about in a regulated manner. For example, blue light-dependent nuclear positioning has been shown in *Arabidopsis* leaf cells (Iwabuchi et al. 2010; Iwabuchi et al. 2007).

Previous studies have revealed that microtubules (MTs) that are connected to the nuclear envelope (NE) are key cytoskeletal players in many animal and yeast cells. Nuclear-attached MTs can move the nucleus via 2 mechanisms. First, the plus end of MTs interacts with the cell cortex and generates either a pushing or pulling force. In fission yeast, centring of the nucleus is achieved through pushing of cell tips by MTs (Tran et al. 2001), whereas cells of budding yeast translocate the nucleus to the bud neck through MT pulling at the cell cortex, near which the minus-end-directed motor called cytoplasmic dynein is concentrated (Adames and Cooper 2000). The second commonly observed mechanism of MT-driven nuclear positioning is dependent on the motor proteins that connect the NE and MTs. For example, female pronuclear movement is caused by nucleus-associated dynein that walks along the MTs coming out of the sperm centrosome (Reinsch and Gonczy 1998). Processive plus-end-directed motors kinesin-1 and kinesin-3 have also been shown to be responsible for nuclear movement; specific proteins at the NE surface recruit these motor proteins (Fridolfsson and Starr 2010; Tsai et al. 2010). In plants, on the other hand, actin and the associated myosin motor protein (e.g. myosin XI-i) control nuclear positioning in many cell types (Chytilova et al. 2000; Iwabuchi et al. 2010; Tamura et al. 2013). Nevertheless, the adaptor proteins on the NE are conserved among yeast, animal, and plant cells; the SUN/KASH protein complex that is embedded in the NE is associated with plant myosin or animal kinesin/dynein (Gundersen and Worman 2013;

Tamura et al. 2013). To our knowledge, kinesin-dependent nuclear translocation has not been identified in land plant cells (note that land plants do not possess cytoplasmic dynein).

The protonemal cell of the moss *Physcomitrella patens* is an emerging model system for plant cell biology, for example, for analysis of the molecular mechanism underlying cell growth and mitosis (Cove 2005; Hiwatashi et al. 2008; Kosetsu et al. 2013; Miki et al. 2014; Nakaoka et al. 2012; Vidali et al. 2007; Vidali et al. 2009). The rate of homologous recombination is unusually high in *P. patens*, so that gene disruption and GFP (or its variant) tagging of the endogenous gene are easy to perform; this approach quickly provides insight into gene functions. As an additional tool for functional studies, we recently developed a conditional RNA interference (RNAi) system, in which a knockdown of a single or multiple homologous genes can be induced in protonemal cells; we used this system to evaluate the effects of downregulation of genes essential for mitosis (Kosetsu et al. 2013; Miki et al. 2014; Nakaoka et al. 2012). Another key feature of the *P. patens* protonemal system is the ease of live cell microscopy. The cells are found in a single layer and actively grow and divide every 5–6 h; thus, they can be studied using high-resolution confocal microscopy and prolonged imaging (>12 h) (Cove 2005; Nakaoka et al. 2012; Prigge and Bezanilla 2010). Combining microscopy and loss-of-function analysis in protonemal cells has provided new insights into gene functions and the molecular mechanisms of certain cellular processes (Augustine et al. 2008; Hiwatashi et al. 2008; Kosetsu et al. 2013; Miki et al. 2014; Nakaoka et al. 2012; Vidali et al. 2007).

Recently, the genome of *P. patens* was analysed, and 78 kinesin superfamily genes were identified (Miki et al. 2014; Shen et al. 2012). Based on the amino acid sequences, *P. patens* kinesin genes were classified into 10 subfamilies. *P. patens* does not possess kinesin-1 or kinesin-3 subfamily genes, which in animal and fungal cells, play a major role in cargo transport, e.g. the nucleus (Hirokawa et al. 2009; Zekert and Fischer 2009). We attached a Citrine tag (a GFP variant) to the C terminus of virtually all kinesins, performed time-lapse microscopy, and identified 43 kinesins associated with the mitotic apparatus such as spindles, phragmoplasts, and chromosomes (Miki et al. 2014). Because most of the kinesins show inconsistent localisation patterns compared to the animal homologues, the function of each kinesin in *P. patens* is not yet clear. Moreover, the study suggested that many kinesins, including the mitotic

kinesins, are also expressed in interphase (Miki et al. 2014); however, the function of these motors in interphase is also unknown.

In this study, we first showed that MTs, but not actin filaments, are required for nuclear centring after cell division in the protonemal cells of *P. patens*. We then performed comprehensive RNAi screening that targeted all 78 kinesins and found that depletion of armadillo repeat-containing kinesins (kinesin-ARKs) affects nuclear positioning. In the absence of kinesin-ARKs, the daughter nucleus in apical cells fails to reach the cell centre and is instead mislocalised to the cell plate-proximal region, concomitantly with the loss of MT bundles around the nucleus. The kinesin-ARK protein is localised to the cytoplasmic MTs *in vivo* and shows MT gliding activity *in vitro*. Taken together, these results suggest that MTs and kinesin-ARK are crucial for nuclear migration.

Results

The nucleus is translocated to the centre in an MT-dependent manner after cell division

In a study by Doonan and colleagues, protonemal apical cells were treated for ≥1 h with an MT-destabilising drug cremart, and the crucial function of MT in tip growth was demonstrated based on the terminal phenotype (Doonan et al. 1988). We repeated this experiment using oryzalin, a compound that has seen frequent usage in recent times (Finka et al. 2007; Hiwatashi et al. 2014), cells expressing GFP-tubulin and histone H2B-mRFP (Nakaoka et al. 2012), and time-lapse imaging along with drug addition. We confirmed the previous finding of the tip growth defect (Finka et al. 2007; Hiwatashi et al. 2014) and observed, as expected, the absence of spindle formation during mitosis (Movie 1). Histone-RFP imaging indicated that the majority of the cells in interphase retain their nuclei in the centre of the cell, while the tip growth was suppressed (Movie 1). During the course of this experiment, we found that nuclear movement just after nuclear division is affected by oryzalin treatment. In control DMSO-treated cells, daughter nuclei were translocated towards the cell centre immediately after cell division (Fig. 1A, D, S1; Movie 2). The nucleus was then kept in the middle of the cell because it was moved towards the cell tip at the rate of tip growth (Fig. S1). In contrast, when oryzalin was added to telophase cells, daughter nuclei were not properly translocated, but rather they stayed at the same position (Fig. 1B, D; Movie 2). This phenomenon was not an indirect effect of the drug on tip growth because treatment with actin inhibitors such as latrunculin B or cytochalasin B (Finka et al. 2007; Harries et al. 2005; Sato et al. 2001; Vidali et al. 2009; Wu and Bezanilla 2014) also suppressed tip growth with no significant effect on nuclear translocation (Fig. 1C, D; Movie 2). These results indicated that nuclear translocation after cell division was dependent, at least partially, on MTs in the apical cell.

RNAi screening identified kinesin-ARKs as the motor proteins required for proper nuclear positioning

The oryzalin experiment suggested that there were at least 3 activities in the protonemal apical cell that required MTs: mitosis, tip growth, and nuclear migration. Because these activities may involve generation of force by motor proteins, we

designed an RNAi screening method to identify kinesin superfamily proteins involved in each process (Fig. 2; Movie 3).

P. patens has 78 kinesins, 69 of which are classified into 10 subfamilies and the remaining 9 are unclassified (Miki et al. 2014). We designed 2 RNAi constructs for each gene. We amplified ~700-bp fragments from the cDNA pool, and cloned them into the pGG626 vector, which is an integration vector for inducible RNAi (Nakaoka et al. 2012). RNAi-pGG626 constructs were introduced into the GFP-tubulin/Histone-RFP cell line, and stable clones were selected. Based on histone-RFP intensity, which is an indicator of RNAi penetrance, we selected ~5 candidate RNAi lines corresponding to each construct (RFP intensity is expected to be reduced concomitantly with a knockdown of the target protein (Nakaoka et al. 2012)). In total, we selected >450 RNAi line, in which 61 genes were targeted. We could not select RNAi lines for the remaining 17 genes mostly because we were unable to amplify these gene fragments. Expression of double-stranded RNAs (dsRNAs) was induced by turning on the promoter using β-estradiol treatment. On days 5–6, time-lapse imaging was performed at 3 min intervals for >6 h, followed by manual examination of the phenotype by watching the cell videos. During analysis of >3,000 movies, we detected defects in mitosis as a result of a knockdown of some genes, such as kinesin-5 or kinesin-7-II subfamily genes (Miki et al. 2014; Naito and Goshima in minor revision). In addition, we observed a specific defect in nuclear positioning in the RNAi lines corresponding to the kinesin-ARK subfamily (Fig. 3, S2).

Kinesin-ARK is a plant-specific subfamily and in *P. patens*, 4 highly homologous genes (*kinesin ARK-a–d*) belong to this subfamily (Fig. S2A, S3). Each member of the kinesin-ARK subfamily has a motor domain at the N terminus and the armadillo repeat motif near the tail region (Fig. S2B). In *Arabidopsis*, a loss of kinesin-ARKs (called ARK1, ARK2, and ARK3) increases MT numbers in root hairs and impairs morphology of root hair cells (Jones et al. 2006; Sakai et al. 2008; Yang et al. 2007). Our previous localisation study suggested that kinesin ARK-a and -b are strongly expressed in protonemal cells, but we detected little or no expression of kinesin ARK-c or -d, respectively (Miki et al. 2014). During mitosis, kinesin ARK-a and -b are located along the spindle and phragmoplast MTs (Miki et al. 2014). Kinesin ARK-a and -b are highly homologous to each other even at the nucleotide sequence level, suggesting that they function redundantly and that an RNAi construct designed

to target one of them is expected to knock both genes down (this was the case for several mitotic genes (Kosetsu et al. 2013; Miki et al. 2014; Nakaoka et al. 2012). We have selected 6 independent stable RNAi lines corresponding to 3 constructs that targeted 2 non-overlapping regions in the *kinesin-ARK* genes (Fig. S2C). Quantitative real-time RT-PCR (qRT-PCR) analysis confirmed that each construct downregulated kinesin ARK-a and -b simultaneously (Fig. S2D). The mRNA level was reduced by >40% in most RNAi lines, with some variability, which is typical of our inducible RNAi system (Kosetsu et al. 2013; Miki et al. 2014; Nakaoka et al. 2012).

An analysis of the time-lapse movies of the 6 RNAi lines did not identify the defects in tip growth or mitotic duration (Fig. S4A, S4B). The overall growth of the protonemata and development of the gametophore, a shoot of moss, were also unaffected (Fig. S4C). However, the caulonemal cells of these lines exhibited a characteristic phenotype (Fig. 3; Movie 4). Mitosis proceeded in exactly the same way as in the control cells, but the daughter nucleus in the apical cell moved back to the cell plate at a very high frequency at the rate of 0.34 ± 0.15 μm/min, while it moved forward in control cells at the rate of 0.31 ± 0.02 μm/min (mean ± SD, between 54 and 81 min in Fig. 3B). The nucleus remained near the cell plate for the next few hours in the RNAi-treated cells.

We investigated the possible effect of actin or MT on the observed backward movement of the nucleus by live cell imaging, combined with the addition of drugs. When the cells were treated with latrunculin B 20–21 min after anaphase, the daughter nucleus of apical cells remained in the control cells. However, they moved back to the cell plate in the absence of kinesin-ARKs (Fig. 4A, B, E; Movie 5). This behaviour was identical to that exhibited by untreated cells (Fig. 3A, B). In sharp contrast, when the cells were treated with oryzalin, the nucleus in the tip cells remained at the same position in both kinesin-ARK RNAi and the control cells (Fig. 4C, D, E; Movie 5). Therefore, we concluded that the backward movement was dependent on MTs, but not on actin.

In RNAi-treated cells, we observed renewed forward movement in the cell plate-proximal nucleus, towards the cell centre 92 ± 34 min (± SD, n = 5) prior to the subsequent mitotic phase at the rate of 0.58 ± 0.45 μm/min (Movie 3; a cell indicated by a white arrow around 5 h 45 min). However, the nuclear position was not fully restored, and we noticed that the mitotic spindle in the RNAi-treated cells was formed at greater proximity to the cell plate, as compared to the control cells (Fig. S5).

Therefore, the ARK subfamily of kinesins and MTs are necessary for nuclear centring, specifically after cell division, which affects the cell division site of subsequent mitosis.

Kinesin-ARKs are associated with MT bundles surrounding the moving nucleus

When high-resolution imaging was performed using confocal microscopy, we identified bundled MTs attached to the moving nucleus in 4 of 5 control cells (Fig. 5A, arrowheads; Movie 6). Such MT bundles, however, were not observed in the RNAi cells (0 of 4 cells). These results suggested that kinesin-ARK protein as a linker connects multiple MTs to the nucleus.

We determined localisation of kinesin ARK-a at the time of nuclear translocation. When the Citrine fusion protein was photographed with mCherry-tubulin, we saw that kinesin ARK-a-Citrine was co-localised with MTs, including those around the nucleus, after chromosome separation (Fig. 5B; Movie 7).

Recently, Eng and Wasteney (2014) reported that *Arabidopsis* ARK1-GFP tracks the growing MT plus-ends in several cell types. Furthermore, ARK1 mutant cells showed reduced MT growing velocity and catastrophe frequency in root hairs. Previous studies in *Arabidopsis* also showed that the growth of the root hair tip is defective due to abnormal abundance of MTs in the endoplasm (Sakai et al. 2008; Yoo et al. 2008). The nuclear migration, however, has not been assessed in those mutants. In order to verify if these results observed in *Arabidopsis* ARK1 would hold true for *P. patens* orthologues, we observed their localisation and dynamics by oblique illumination fluorescence microscopy. This method allowed clear visualisation of individual MTs near the cell membrane because of the reduced background signals (Konopka and Bednarek 2008; Tokunaga et al. 2008) (note that the nucleus and the surrounding MTs could not be observed because they were located too far away from the cell cortex). This method confirmed that kinesin ARK-a-Citrine and ARK-b-Citrine are localised along growing and shrinking MTs in the cytoplasm, and are not limited to the growing plus-ends (Fig. S6; Movie 8). We observed that the Citrine signals, which may have corresponded to the clustered kinesins, did not move along the MT (the microscope used was not sensitive enough to detect a single Citrine molecule *in vivo*). Time-lapse imaging of the GFP-tubulin indicated no changes in the MT growth rate in kinesin-ARK RNAi cells (Fig. S7A). Due to the growth of the MTs beyond the imaging field, we were unable to measure the catastrophe frequency.

However, we also observed, through immunofluorescence microscopy of the MTs, that the overall MT abundance remained unaltered in the absence of kinesin-ARK (Fig. S7B).

These results suggest that kinesin-ARK plays little role in the regulation of MT dynamics in protonemal cells. This situation could be due to an inefficient knockdown of kinesin-ARKs in the system, or differences among the cell types. Alternately, *Arabidopsis* ARKs might have acquired a new function during evolution.

Kinesin-ARK-a possesses a plus-end-directed motor activity

The motor activity of kinesin-ARKs has not been characterised in previous studies. To test whether *P. patens* kinesin-ARKs have the plus-end-directed motor activity, we performed an MT-gliding assay using the purified truncated kinesin ARK-a that possesses the motor and dimerisation domains (64–482 a.a.; Fig. 6A, B; the domain organisation is highly conserved among kinesin ARK-a–d). In this assay, kinesin motors tagged with GFP were bound to the glass surface via an anti-GFP antibody, and fluorescently labelled MTs near the glass surface were examined under a total internal reflection fluorescence microscope (TIRFM). In the presence of ATP, we observed MT gliding at the rate of 11.7 ± 7.1 μm/min (~200 nm/sec; mean ± SD), whereas the motion was not observed when ATP was replaced with AMP-PNP, a non-hydrolysable analogue of ATP (Fig. 6C; Movie 9). Finally, to assess directionality of the motor, we utilised polarity-marked MTs in a gliding assay. The imaging data indicated that the kinesin ARK-a motor exhibited plus-end-directed motility exclusively (n = 42 MTs; Fig. 6D, E). We concluded that kinesin ARK-a is an MT plus-end-directed motor protein.

Discussion

This study is focused on nuclear positioning, an intracellular process generally believed to be actin dependent in plant cells (Chytilova et al. 2000; Iwabuchi et al. 2010; Tamura et al. 2013). Our data demonstrate that MTs and an MT-based motor protein –the ARK kinesin subfamily– are necessary for proper positioning of the nucleus in the tip-growing protonemal apical cells of the moss *P. patens* (Fig. 7). The strongest evidence supporting this notion is that the centring of a daughter nucleus at the end of cell division is perturbed by either an MT-destabilising drug or an RNAi knockdown of a potent motor protein, kinesin-ARK. Nuclear translocation in other phases is also shown to require MTs, but not kinesin-ARKs. On the other hand, our results suggest that actin and myosin play little role in the nuclear positioning process in these cells.

Mechanism of kinesin-ARK-mediated nuclear positioning

How does kinesin-ARK drive nuclear positioning? One possibility is that kinesin-ARK works rather indirectly. The tail domain of *Arabidopsis* ARK is known to bind to the NIMA-related kinase *in vitro* (Sakai et al. 2008) and ARK1 genetically interacts with AGD1, a class I adenosine diphosphate (ADP) ribosylation factor GTPase-activating protein (ARF-GAP) (Yoo and Blancaflor 2013; Yoo et al. 2008). These signalling molecules might control nuclear positioning via an unknown mechanism. Alternatively, kinesin-ARK may regulate MT dynamics and thereby alter MT's pushing/pulling force applied to the cell plate; this mechanism might in turn affect forces acting on the nucleus, which associates with the MTs. However, we did not observe aberrations in MT dynamics or MT numbers. Therefore, while the above explanations cannot be ruled out, perhaps the most likely scenario is the following: the kinesin-ARK protein transports the nucleus as a cargo, just like kinesins and dynein in animal cells and myosin XI in *Arabidopsis* do. The plus-end-directed motor activity of kinesin-ARK and the MT orientation in the apical cell are consistent with this scenario. In protonemal apical cells, MTs are aligned longitudinally throughout the cytoplasm (Doonan et al. 1985). The majority of growing plus ends moves to the apical side in the apical region of the cells, whereas MTs display a mixed polarity in the basal region (i.e., behind the nucleus) (Hiwatashi et al. 2014). An efficient way to transport the

nucleus to the apical side would be to use the plus-end-directed kinesins on the uniformly oriented MTs. In this scenario, it is expected that MTs are laterally associated with the nuclear surface during the migration. Indeed, around the migrating nucleus, we frequently observe MT bundles that form in a kinesin-ARK-dependent manner, and the motor protein is associated with those bundles. The key to proving this mechanism is to identify the adaptor protein that bridges the NE and the kinesin-ARK motor.

Kinesin-ARK is localised along the endoplasmic MT

We have demonstrated that the kinesin-ARK motor protein has an MT-gliding activity *in vitro*. In protonemal cells, it was localised on MTs. However, we did not detect motility of the punctate kinesin-ARK-Citrine signals along the MT near the cell cortex. Lack of motility *in vivo* may be due to this kinesin having a non-processive motor domain (i.e. performing only one step before dissociation). Alternatively, the kinesin-ARK identified on the MTs may be present in an inactive form, and motility may not be observed unless a cargo binds to the kinesin. In fact, the cargo-dependent activation is a commonly observed characteristic of kinesin family proteins (Verhey and Hammond 2009). If the nucleus were the cargo of kinesin-ARK, the non-motility of this motor near the cortex would make sense, as the nucleus is located more towards the interior of the cell. However, Citrine fusion to the kinesin attenuated functionality is a possibility that cannot be excluded, although *Arabidopsis* ARK1 was proven to be functional despite GFP-tagging at the C terminus (Eng and Wasteneys 2014).

Nuclear positioning in the protonemal apical cell cycle

Our data are also suggestive of the presence of 4 force-generating mechanisms acting on the nucleus in apical cells. First, we observe forward movement during cytokinesis (Fig. 3B, 3–21 min; Fig. 7, phase I). This movement is MT-dependent, since it was inhibited when oryzalin was added to the telophase cell (Fig. 1). Second, the nucleus migrates a short distance towards the cell plate (Fig. 3B, 24–51 min; Fig. 7, phase II). This movement was also dependent on MT, but independent of actin (Fig. 4). Considering the MT orientation in the apical cell (Hiwatashi et al. 2014), a possible explanation is that the nucleus is transported by a minus-end-directed kinesin. Third, the nucleus is moved to the centre of the cell by the action of MTs and kinesin-ARKs, which might transport the nucleus as a cargo (Fig. 3B, 54-81 min; Fig. 7, phase III). If

this were the case, however, we might also postulate the presence of opposing motors or MAPs on the nucleus and/or cytoplasmic viscoelasticity, since the rate of nuclear migration was much lower than the MT gliding velocity of the kinesin-ARK motor domain. Finally, we found that a nucleus that is aberrantly located near the basal side – in the absence of kinesins of the ARK subfamily – eventually migrates, albeit not completely, to the middle region of the apical cell before subsequent mitosis (Movie 3; Fig. 7, phase IV). This pattern of migration is reminiscent of that observed in subapical cells, where the MT-dependent mechanism places the nucleus at the neck of side branches prior to mitosis (Doonan et al. 1986). An unidentified plus-end-directed kinesin or global reorganisation of MTs might be involved in this type of migration.

Conclusions

This study provides a new mechanistic view of nuclear positioning in plant cells, namely, the nucleus may be driven by an MT- and kinesin-dependent mechanisms. This finding suggests that the intrinsic mechanisms underlying this process are widely conserved among fungal, animal, and plant species; which mechanism predominates depends on the cell type. Indeed, actomyosin systems also contribute to nuclear movement in animal cells (Gundersen and Worman 2013; Norden et al. 2009). Whether flowering plants generally possess a similar MT- and kinesin-dependent mechanism has yet to be determined. Intriguingly, MTs were shown to be necessary for prevention of the actin-dependent mechanism of nuclear migration in the root hair of a legume species (Lloyd et al. 1987). It would be interesting to evaluate the contribution of kinesin-ARK to this and other processes in flowering plants.

Materials and methods

Moss culture, RNAi, and transformation

For moss culture and transformation, we essentially followed the methods described in (Nakaoka et al. 2012). In brief, BCDAT medium on which cellophane (a gift of Futamura Chemical Industries) was placed was used for regular culturing of protonemata at 25° C under continuous white light. Transformation was performed by the standard polyethylene glycol-mediated method using the protoplast (driselase [Kyowa Hakko Kogyo] was used for cell wall digestion). To observe RNAi phenotypes, we cultured protonemata for 5–6 days in the presence of 1 μM β-estradiol that turns on the promoter (Kubo et al. 2013) and thereby expression of dsRNAs. Protonemal cells, which had been cultured on 35 mm glass-bottom dish (MatTek) or 6-well glass-bottom plate (IWAKI) with BCD agar medium at 24–25°C, were imaged. In the RNAi screening, we prepared a control GFP-tubulin/HistoneH2B-mRFP line and 5 RNAi lines each time, and imaged a total of ~30 sites every 3 min for >6 h.

Plasmids and moss lines

The background strain of all moss lines used in this study was the Gransden 2004 line obtained from M. Hasebe (NIBB, Japan). GFP-tubulin/HistoneH2B-mRFP (Nakaoka et al. 2012) and kinesin-ARK-Citrine/mCherry-tubulin lines (Miki et al. 2014) have been previously described. In brief, the GFP-tubulin construct contains the rice actin promoter, *sGFP*, the *α*-tubulin gene (AB096718), an rbcS terminator, a G418-resistant cassette, and the *HB7*-target site (Hiwatashi et al. 2008). The HistoneH2B-mRFP construct contains the 7113 promoter (Mitsuhara et al. 1996), human *HistoneH2B* gene, *mRFP* gene, the terminator sequence of the *Agrobacterium tumefaciens* nopaline synthase, a zeocin-resistant cassette, and the 213 gene-targeting site (Nakaoka et al. 2012). The mCherry-tubulin construct contains the rice actin promoter, the *mCherry* gene, an α-tubulin gene, an rbcS terminator, a hygromycin-resistant cassette, and the *PIG1*-target site (Miki et al. 2014). In order to obtain kinesin-ARK-Citrine lines, integration plasmids were constructed, where the Citrine was fused to the C terminus of kinesin-ARK. The ~1 kb C terminus and ~1 kb 3′-untranslated region (UTR) sequences of the kinesin-ARK genes were flanked by the *Citrine* gene, the terminator

sequence from the *Agrobacterium tumefaciens* nopaline synthase, and a G418-resistant cassette (Miki et al. 2014). Kinesin RNAi constructs were obtained using the Gateway system (Invitrogen) with pGG626 (Nakaoka et al. 2012) as the destination vector. The probable gene targeting site of pGG626 is the *PIG1* locus, but the actual integration site(s) were not verified. PCR primers used for RNAi are listed in Table S1.

Microscopy, drug treatment, and immunostaining

For the imaging of drug-treated cells and long-term imaging of the RNAi lines, fluorescence imaging was performed with Nikon's Ti microscope (20× 0.75-NA (drug treatment), 10× 0.45-NA or 10× 0.50-NA (RNAi screening) lens) equipped with an electron-multiplying charge-coupled device (EMCCD) camera (Evolve; Roper, or iXon3; Andor) or Nikon's TE2000 microscope (10× 0.30-NA lens) equipped with an EMCCD camera (Micromax; Roper). Images were acquired every 1 or 3 min (drug treatment) or at multiple sites every 3 min (RNAi screening). For the high-magnification, time-lapse microscopy of the kinesin-Citrine or RNAi lines, the Nikon TE2000 microscope equipped with the spinning-disc confocal unit CSU-X1 (Yokogawa) and an EMCCD camera (ImagEM; Hamamatsu) was used (100× 1.40-NA, 60× 1.40-NA or 40× 1.30-NA lens). A 1.5× intermediate magnification lens was also used for the observation of MT dynamics. Images were acquired every 3 s (for MT dynamics), 0.5 min, or 1 min. For *in vivo* oblique illumination microscopy or *in vitro* TIRFM assay, Nikon's Ti microscope (100× 1.49-NA lens) equipped with an EMCCD camera (Evolve; Roper) and 488/561-nm excitation laser was used. A 2.5× intermediate magnification lens was also used for the *in vivo* observation. Images were acquired every 3 sec (*in vivo*) or 1 sec (*in vitro*). The microscopes were controlled by the Micro-Manager software (Edelstein et al. 2010) and image data were analysed with ImageJ. In RNAi screening, we inoculated a piece of the protonemata onto a thin layer of BCD agar medium prepared in a 6-well glass-bottom plate. To prevent the agar pad drying up, the plate was soaked with ~1 mL water > 1 h prior to imaging. Drug treatment was performed by addition of 1.5 mL water immediately before observation, and 0.5 mL drug solution to the plate at 5–6 min or 20–21 min after the onset of anaphase. The stock drug solutions were prepared as follows: 20 mM oryzalin (AccuStandard) in DMSO, 25 mM latrunculin B (AdipoGen) in DMSO, and 20 mM cytochalasin B (Wako) in DMSO. Cells were treated with 10 µM oryzalin (0.05% DMSO), 25 µM latrunculin B (0.1% DMSO), 200 µM cytochalasin B (1.0% DMSO),

or, as control, 0.5% or 1.0% DMSO only. Immunostaining of MTs was performed basically as described (Nakaoka et al. 2012). In brief, cells were cultured for 6 days in a 35 mm glass-bottom dish on which a thin layer of the BCD agar medium was placed. MT was stained with the DM1A antibody (1:500).

Quantitative real-time RT-PCR (qRT-PCR)

The method is essentially described in (Miki et al. 2014). In brief, RNA was prepared from protonemal cells using the RNeasy Plant Mini Kit (QIAGEN). cDNA was synthesised with the PrimeScript II 1st strand cDNA Synthesis Kit (TAKARA). qRT-PCR was performed in triplicate using Power SYBR Green PCR Master Mix and the 7500 Real-Time PCR system (model 7500; Applied Biosystems). The results were normalized to those for *TUA1* (α-tubulin) (Miki et al. 2014; Nakaoka et al. 2012). Primers for qRT-PCR are listed in Table S1.

Sequence analysis and gene ID

We followed the method described in (Miki et al. 2014). The deduced amino acid sequences were aligned using MAFFT ver. 7.043 (Katoh et al. 2002; Katoh and Standley 2013) and revised manually with MacClade ver. 4.08 OS X. In Fig. 3A, 641 amino acid residues were used to calculate evolution distances for 9 genes using the JTT model (Jones et al. 1992) to construct a neighbour-joining tree by the MEGA5 software (Tamura et al. 2011). Statistical support for internal branches by bootstrap analyses was calculated using 1,000 replications. Kinesin-ARKs of the other species were obtained by the BLASTP search using the amino acid sequence of Pp Kinesin ARK-a as the query. The Arabidopsis Information Resource (http://www.arabidopsis.org) and Phytozome (http://www.phytozome.net) (for *Selaginella moellendorffii*) were used as the database. Gene IDs are as follows. Pp *kinesin ARK-a* (Phypa_455498/Pp1s280_66V6), Pp *kinesin ARK-b* (Phypa_453488/Pp1s242_11V6), Pp *kinesin ARK-c* (Phypa_ 425827/Pp1s14_211V6), Pp *kinesin ARK-d* (Phypa_ 427907/Pp1s22_256V6), At *Ark-1* (AT3G54870), At *Ark-2* (AT1G01950), At *Ark-3* (AT1G12430).

Protein purification

The motor and dimerisation domains of kinesin ARK-a were fused with mGFP and 6×His, and cloned into an *E. coli* expression vector pET23a (Novagen). Primers listed

in Table S1 were used for PCR, and cloning was performed with *HindIII/XhoI* digestion of pTM475 (mGFP-6×His), with subsequent NdeI/NotI digestion of the pGG886 (Kinesin-ARK-a-motor-mGFP-6×His) plasmid. The resultant plasmid pGG886 was transformed into *E. coli* SoluBL21 strain (Genlantis). Proteins were expressed at 18˚C with 0.2 mM IPTG. Bacterial pellet from 250 mL culture was homogenised with a homogeniser (Branson-Emerson Sonifier 250D-Advanced; BRANSON)) in lysis buffer (50 mM $NaPO_4$, pH 8.0, 250 mM NaCl, 2 mM $MgCl_2$, 20 mM imidazole, 10 mM 2-mercaptoethanol, 1 mM ATP, protease inhibitors). Post-centrifugation, the supernatant of the bacterial extract was incubated with Ni-NTA resin for 2 h at 4˚C. The Ni-NTA resin was washed with wash buffer (50 mM $NaPO_4$, pH 6.0, 250 mM NaCl, 1 mM $MgCl_2$, 60 mM imidazole, 10 mM 2-mercaptoethanol, 0.1 mM ATP) followed by purification with Ni-NTA resin and elution buffer (50 mM $NaPO_4$, pH 7.2, 250 mM NaCl, 1 mM $MgCl_2$, 500 mM imidazole, 10 mM 2-mercaptoethanol, 0.1 mM ATP). The buffer was exchanged to BRB80 (80 mM K-PIPES, pH 6.8, 2 mM $MgCl_2$, 1 mM EGTA) containing 10 mM 2-mercaptoethanol and 0.1 mM ATP by PD MiniTrap G-25 (GE Healthcare). The protein was further affinity-purified using taxol-stabilised MTs and 1 mM AMP-PNP. The mixture was centrifuged at 80,000 g for 15 min at 25 ˚C, followed by release of the active motor with 5 mM ATP. The MT gliding assay was performed immediately after protein purification.

MT gliding assay

The conventional MT gliding assay (Woehlke et al. 1997) was performed with some modifications. Flow chambers were assembled between a silanised coverslip and a microslide glass with double-sided sticky tape. The coverslip was coated with the anti-GFP antibody (rabbit polyclonal, affinity-purified). The chamber was washed with BRB80 and purified GFP-tagged kinesin ARK-a motor was flowed into the chamber. After washed with BRB80 containing 0.5 mg/ml k-casein, the motility buffer (BRB80, GMP-CPP-stabilised MTs with Alexa 568-labels, 2 mM ATP or AMP-PNP, 0.5 mg/ml k-casein, and 0.1% methylcellulose, 20 μM taxol with oxygen scavenger system (50 mM glucose, 400 μg/ml glucose-oxidase, 200 μg/ml catalase, and 4 mM DTT) (Li et al. 2012)) was flowed into the chamber. For polarity-marked and GMP-CPP-stabilised MTs preparation, bright MTs seeds (80% unlabelled tubulin: 20% Alexa 568-labelled tubulin) were first assembled, followed by polymerisation of

dim MTs (67% unlabelled tubulin: 2% Alexa 568-labelled tubulin: 31% *N*-ethylmaleimide (NEM) tubulin. Imaging was performed with total internal reflection fluorescence microscope (TIRFM), and the gliding velocity was measured with kymographs.

Funding Statement

This work was supported by the Next Generation grant (Japan Society for Promotion of Science; JSPS), James A. and Faith Miller Memorial Fund, and Human Frontier Science Program (to G.G.). T.M. is a recipient of a pre-doctoral fellowship of the JSPS.

Disclosures

All authors declare that there are no conflicts of interest.

Acknowledgements

We thank Drs. Erik Jonsson, Ronald Vale, Michio Tomishige, Tomoko Nishiyama, Takashi Moriwaki, and Yuki Nakaoka for technical advice and reagents; Dr. Yasunori Machida, Ms. Rie Inaba, and Ms. Ayako Watanabe for technical assistance.

Author contributions

T.M. and G.G. designed the research project; T.M., M.N., and G.G. performed the experiments; T.M., M.N., and G.G. analysed the data; T.M. and G.G. wrote the manuscript.

Supplementary information

Figure S1. Position of the nucleus during the protonemal cell cycle

(**A**) Imaging of GFP-tubulin (green) and HistoneH2B-mRFP (red) in the cell cycle of a protonemal apical cell. The mitotic spindle (58 min) and the phragmoplast (83 min) were detected during mitosis. (**B**) A kymograph showing the position of the nucleus relative to the cell tip. During most of the interphase, the nucleus moves forward, such that it is retained in the centre of the cell. Bars, 50 µm.

Figure S2. RNAi knockdown of kinesins of the ARK subfamily

(**A**) Phylogenetic analysis of the kinesin-ARK subfamily of kinesins from *Physcomitrella patens* (Pp), *Arabidopsis thaliana* (At), and *Selaginella moellendorffii* (Sm). The numbers near the branches represent local bootstrap probability. The local bootstrap values (1,000 replicates) are also shown near the branches. The horizontal branch length is proportional to the estimated evolutionary distance. Kinesin-ARKs from *Selaginella moellendorffii* were provisionally named based on the accession numbers in the Phytozome database. A bar indicates an amino acid substitution per site. *P. patens* expresses another ARK-like kinesin (Miki et al. 2014; Shen et al. 2012). However, this protein was excluded from our analysis because only the motor domain was identified. (**B**) Illustration of the structure of kinesins from the ARK subfamily. They contain the kinesin motor domain, the coiled-coil domain, and the armadillo repeat (marked with 'A'). The Simple Modular Architecture Research Tool (SMART) software (EMBL) was used in the identification of each domain. (**C**) Three RNAi constructs were used for the downregulation of kinesin-ARKs. Grey and red bars indicate cDNAs and dsRNAs, respectively. The (%) values indicate nucleotide sequence homology. (**D**) Quantitative real-time RT-PCR (qRT-PCR) confirmed a successful knockdown of kinesins ARK-a and -b. The values, relative to the control cell clone (set to 1.0), are plotted as mean ± SEM from 2 independent experiments.

Figure S3. Amino acid sequence alignment of 4 *P. patens* kinesin-ARKs

The Clustal Omega program (EMBL) was used.

Figure S4. Protonemal growth, mitosis duration, or gametophore formation is

not perturbed by kinesin-ARK RNAi

(**A**) The tip growth velocity of caulonemal apical cells was measured by time-lapse imaging. The mean values of the growth rate obtained in 3–7 independent experiments are shown with SEM. No statistically significant differences were observed for RNAi-treated cells (line #7, p= 0.40; line #9, p = 0.93 (t-test)). (**B**) Nuclear envelope breakdown (NEBD)-to-anaphase duration was not significantly altered following RNAi (mean ± SEM). Control, n = 52; kinesin-ARK RNAi 1st construct, line #7, n = 19, p = 0.88 (t-test); line #8, n = 9, p = 0.16; 2nd construct, line #7, n = 31, p = 0.72; line #9, n = 33, p = 0.25; 3rd construct, line #2, n = 10, p = 0.57; line #3, n = 18, p = 0.83. (**C**) Each clone was cultured for 3 weeks in the BCDAT agar medium with 1 μM β-estradiol. The PpXMAP215 RNAi line, which shows a severe growth defect of protonemata, was used as a control (Nakaoka et al. 2012). Bar, 1 cm.

Figure S5. The spindle positioning defect after kinesin-ARK RNAi

The relative position of the mitotic spindle in the apical cell was measured. The representative control and kinesin-RNAi cells (1st construct, line #8, and 2nd construct, line #9) have been displayed. The quantitative data has also been plotted (error bars represent SEM). Control, n = 29; kinesin-ARK RNAi 1st construct, line #7, n = 11; line #8, n = 4, 2nd construct, line #7, n = 14; line #9, n = 15; 3rd construct, line #2, n = 5; line #3, n = 10). The relative spindle position in kinesin-ARK RNAi cells is significantly different from that in the control cells (t-test). 1st construct, line #7, p = 0.001; line #8, p = 0.003, 2nd construct, line #7, p = 0.0002; line #9, p < 0.0001, and 3rd construct, line #2, p < 0.0001; line #3, p = 0.0007. Bar, 100 μm.

Figure S6. Localisation of kinesin ARK-Citrine on growing and shrinking MTs

This figure represents the time-lapse images of cells expressing mCherry-tubulin and kinesin ARK-b-Citrine by oblique illumination fluorescence microscopy. Localisation of kinesin ARK-b-Citrine along the cytoplasmic MT was observed. See also Movie 9. Bar, 10 (upper) or 5 μm (bottom).

Figure S7. Kinesin-ARK RNAi does not affect the growth rate or abundance of endoplasmic MTs

(**A**) The MT growth rate was not significantly different between control and

kinesin-ARK RNAi cells near the cell surface. GFP-tubulin was imaged every 3 s by spinning-disc confocal microscopy, and the kymographs were analysed. Mean ± SEM is plotted (25 MTs of 5 cells for each line). The p-values based on Student's t-test were, 0.24 for the 1st construct, line #7; 0.49 for line #8; 0.85 for the 2nd construct, line #7; 0.76 for line #9; 0.83 for the 3rd construct, line #2; 0.69 for line #3. (**B**) Mean fluorescent intensity of MTs in the endoplasmic region. MTs were stained with the anti-tubulin antibody. The locations, 25 μm and 50 μm from the tip, were measured (mean ± SEM, each n = 5). The representative MT network of a control cell, observed by spinning-disc confocal microscopy is also displayed. Bar, 50 μm.

Table S1. PCR primers used in kinesin RNAi screening

Listed in a separate MS Word file.

Movie 1. Effect of oryzalin on protonemal cells

Time-lapse imaging (wide-field microscopy) of protonemal cells expressing GFP-tubulin (green) and HistoneH2B-mRFP (red). Oryzalin (10 μM) was added at time 0. Note that chromosomes are scattered in the cytoplasm when the cells enter mitosis without spindle formation. Bar, 100 μm.

Movie 2. MT-dependent nuclear movements at the end of cell division

Time-lapse imaging (wide-field microscopy) of caulonemal cells expressing GFP-tubulin (green) and HistoneH2B-mRFP (red). DMSO, oryzalin, or latrunculin B was added at 5−6 min. Bar, 100 μm.

Movie 3. Kinesin RNAi screening by using live cell microscopy of protonemal cells

Time-lapse imaging (wide-field microscopy) of protonemal cells expressing GFP-tubulin (green) and HistoneH2B-mRFP (red). In this example (kinesin-ARK RNAi), aberrations in nuclear migration were observed (blue arrows). Nonetheless, prior to mitosis, the nucleus moved to the centre of the cell (white arrowhead at 5 h 33 min to 6 h 03 min). Control cells are also displayed (yellow arrows indicate normal nuclear movement). Bar, 100 μm.

Movie 4. Kinesin-ARK-dependent nuclear movements at the end of cell division according to low-magnification imaging

Time-lapse imaging (wide-field microscopy) of caulonemal cells expressing GFP-tubulin (green) and HistoneH2B-mRFP (red). Bar, 100 µm.

Movie 5. Abnormal migration of the nucleus in the absence of kinesin-ARK depends on MTs, but not on actin

Time-lapse imaging (wide-field microscopy) of caulonemal cells expressing GFP-tubulin (green) and HistoneH2B-mRFP (red). Oryzalin or latrunculin B was added at 20−21 min in the control or kinesin-ARK RNAi cells. Bar, 100 µm.

Movie 6. Kinesin-ARK-dependent nuclear movements at the end of cell division according to high-resolution imaging

Time-lapse imaging (spinning-disc confocal microscopy) of caulonemal cells expressing GFP-tubulin (green) and HistoneH2B-mRFP (red). Bar, 10 µm.

Movie 7. Localisation of kinesin ARK-a-Citrine on MTs at the end of cell division

Time-lapse imaging (spinning-disc confocal microscopy) of a caulonemal cell expressing kinesin ARK-a-Citrine (green) and mCherry-tubulin (red). A cell without Citrine expression is shown as a control in the bottom panels; note the autofluorescence derived from chloroplasts. Bar, 10 µm.

Movie 8. Localisation of kinesin ARK-a and -b on growing and shrinking MTs

Time-lapse imaging of a protonemal cell expressing Citrine-tagged kinesin-ARKs (green) and mCherry-tubulin (red). Images were acquired every 3 s by oblique illumination fluorescence microscopy. Bar, 10 µm.

Movie 9. *In vitro* activity of kinesin-ARK

An MT gliding assay (in the presence of ATP or AMP-PNP) involving the purified motor protein kinesin ARK-a. The video is repeated 3 times. Bar, 10 µm.

References

Adames, N.R. and Cooper, J.A. (2000) Microtubule interactions with the cell cortex causing nuclear movements in Saccharomyces cerevisiae. *J Cell Biol* 149: 863-874.

Augustine, R.C., Vidali, L., Kleinman, K.P. and Bezanilla, M. (2008) Actin depolymerizing factor is essential for viability in plants, and its phosphoregulation is important for tip growth. *Plant J* 54: 863-875.

Chytilova, E., Macas, J., Sliwinska, E., Rafelski, S.M., Lambert, G.M. and Galbraith, D.W. (2000) Nuclear dynamics in Arabidopsis thaliana. *Mol Biol Cell* 11: 2733-2741.

Cove, D. (2005) The moss Physcomitrella patens. *Annu Rev Genet* 39: 339-358.

Doonan, J.H., Cove, D.J. and Lloyd, C.W. (1985) Immunofluorescence microscopy of microtubules in intact cell lineages of the moss, Physcomitrella patens. I. Normal and CIPC-treated tip cells. *J Cell Sci* 75: 131-147.

Doonan, J.H., Cove, D.J. and Lloyd, C.W. (1988) Microtubules and microfilaments in tip growth: evidence that microtubules impose polarity on protonemal growth in Physcomitrella patens. *J Cell Sci* 89: 533-540.

Doonan, J.H., Jenkins, G.I., Cove, D.J. and Lloyd, C.W. (1986) Microtubules connect the migrating nucleus to the prospective division site during side branch formation in the moss Physcomitrella patens. *Eur J Cell Biol* 41: 157-164.

Edelstein, A., Amodaj, N., Hoover, K., Vale, R. and Stuurman, N. (2010) Computer control of microscopes using μManager. *Curr Protoc Mol Biol* Chapter 14: Unit14 20.

Eng, R.C. and Wasteneys, G.O. (2014) The Microtubule Plus-End Tracking Protein ARMADILLO-REPEAT KINESIN1 Promotes Microtubule Catastrophe in Arabidopsis. *Plant Cell* 26: 3372-3386.

Finka, A., Schaefer, D.G., Saidi, Y., Goloubinoff, P. and Zryd, J.P. (2007) In vivo visualization of F-actin structures during the development of the moss Physcomitrella patens. *New Phytol* 174: 63-76.

Fridolfsson, H.N. and Starr, D.A. (2010) Kinesin-1 and dynein at the nuclear envelope mediate the bidirectional migrations of nuclei. *J Cell Biol* 191: 115-128.

Gundersen, G.G. and Worman, H.J. (2013) Nuclear positioning. *Cell* 152: 1376-1389.

Harries, P.A., Pan, A. and Quatrano, R.S. (2005) Actin-related protein2/3 complex component ARPC1 is required for proper cell morphogenesis and polarized cell growth in Physcomitrella patens. *Plant Cell* 17: 2327-2339.

Hirokawa, N., Noda, Y., Tanaka, Y. and Niwa, S. (2009) Kinesin superfamily motor proteins and intracellular transport. *Nat Rev Mol Cell Biol* 10: 682-696.

Hiwatashi, Y., Obara, M., Sato, Y., Fujita, T., Murata, T. and Hasebe, M. (2008) Kinesins are indispensable for interdigitation of phragmoplast microtubules in the moss Physcomitrella patens. *Plant Cell* 20: 3094-3106.

Hiwatashi, Y., Sato, Y. and Doonan, J.H. (2014) Kinesins have a dual function in organizing microtubules during both tip growth and cytokinesis in Physcomitrella patens. *Plant Cell* 26: 1256-1266.

Iwabuchi, K., Minamino, R. and Takagi, S. (2010) Actin reorganization underlies phototropin-dependent positioning of nuclei in Arabidopsis leaf cells. *Plant Physiol* 152: 1309-1319.

Iwabuchi, K., Sakai, T. and Takagi, S. (2007) Blue light-dependent nuclear positioning in Arabidopsis thaliana leaf cells. *Plant Cell Physiol* 48: 1291-1298.

Jones, D.T., Taylor, W.R. and Thornton, J.M. (1992) The rapid generation of mutation data matrices from protein sequences. *Comput Appl Biosci* 8: 275-282.

Jones, M.A., Raymond, M.J. and Smirnoff, N. (2006) Analysis of the root-hair

morphogenesis transcriptome reveals the molecular identity of six genes with roles in root-hair development in Arabidopsis. *Plant J* 45: 83-100.
Katoh, K., Misawa, K., Kuma, K. and Miyata, T. (2002) MAFFT: a novel method for rapid multiple sequence alignment based on fast Fourier transform. *Nucleic Acids Res* 30: 3059-3066.
Katoh, K. and Standley, D.M. (2013) MAFFT multiple sequence alignment software version 7: improvements in performance and usability. *Mol Biol Evol* 30: 772-780.
Konopka, C.A. and Bednarek, S.Y. (2008) Variable-angle epifluorescence microscopy: a new way to look at protein dynamics in the plant cell cortex. *Plant J* 53: 186-196.
Kosetsu, K., de Keijzer, J., Janson, M.E. and Goshima, G. (2013) MICROTUBULE-ASSOCIATED PROTEIN65 is essential for maintenance of phragmoplast bipolarity and formation of the cell plate in Physcomitrella patens. *Plant Cell* 25: 4479-4492.
Kubo, M., Imai, A., Nishiyama, T., Ishikawa, M., Sato, Y., Kurata, T., et al. (2013) System for Stable β -Estradiol-Inducible Gene Expression in the Moss Physcomitrella patens. *PLoS One* 8: e77356.
Li, W., Moriwaki, T., Tani, T., Watanabe, T., Kaibuchi, K. and Goshima, G. (2012) Reconstitution of dynamic microtubules with Drosophila XMAP215, EB1, and Sentin. *J Cell Biol* 199: 849-862.
Lloyd, C.W., Pearce, K.J., Rawlins, D.J., Ridge, R.W. and Shaw, P.J. (1987) Endoplasmic microtubules connect the advancing nucleus to the tip of legume root hairs, but F-actin is involved in basipetal migration. *Cell Motil Cytoskeleton* 8: 27-36.
Miki, T., Naito, H., Nishina, M. and Goshima, G. (2014) Endogenous localizome identifies 43 mitotic kinesins in a plant cell. *Proc Natl Acad Sci U S A* 111: E1053-1061.
Mitsuhara, I., Ugaki, M., Hirochika, H., Ohshima, M., Murakami, T., Gotoh, Y., et al. (1996) Efficient promoter cassettes for enhanced expression of foreign genes in dicotyledonous and monocotyledonous plants. *Plant Cell Physiol* 37: 49-59.
Naito, H. and Goshima, G. (in minor revision) NACK kinesin is required for metaphase chromosome alignment and cytokinesis in the moss Physcomitrella patens. *Cell Struct Funct*.
Nakaoka, Y., Miki, T., Fujioka, R., Uehara, R., Tomioka, A., Obuse, C., et al. (2012) An inducible RNA interference system in Physcomitrella patens reveals a dominant role of augmin in phragmoplast microtubule generation. *Plant Cell* 24: 1478-1493.
Norden, C., Young, S., Link, B.A. and Harris, W.A. (2009) Actomyosin is the main driver of interkinetic nuclear migration in the retina. *Cell* 138: 1195-1208.
Prigge, M.J. and Bezanilla, M. (2010) Evolutionary crossroads in developmental biology: Physcomitrella patens. *Development* 137: 3535-3543.
Reinsch, S. and Gonczy, P. (1998) Mechanisms of nuclear positioning. *J Cell Sci* 111 (Pt 16): 2283-2295.
Sakai, T., Honing, H., Nishioka, M., Uehara, Y., Takahashi, M., Fujisawa, N., et al. (2008) Armadillo repeat-containing kinesins and a NIMA-related kinase are required for epidermal-cell morphogenesis in Arabidopsis. *Plant J* 53: 157-171.
Sato, Y., Wada, M. and Kadota, A. (2001) Choice of tracks, microtubules and/or actin filaments for chloroplast photo-movement is differentially controlled by phytochrome and a blue light receptor. *J Cell Sci* 114: 269-279.
Shen, Z., Collatos, A.R., Bibeau, J.P., Furt, F. and Vidali, L. (2012) Phylogenetic analysis of the Kinesin superfamily from physcomitrella. *Front Plant Sci* 3: 230.
Tamura, K., Iwabuchi, K., Fukao, Y., Kondo, M., Okamoto, K., Ueda, H., et al. (2013)

Myosin XI-i links the nuclear membrane to the cytoskeleton to control nuclear movement and shape in Arabidopsis. *Curr Biol* 23: 1776-1781.
Tamura, K., Peterson, D., Peterson, N., Stecher, G., Nei, M. and Kumar, S. (2011) MEGA5: molecular evolutionary genetics analysis using maximum likelihood, evolutionary distance, and maximum parsimony methods. *Mol Biol Evol* 28: 2731-2739.
Tokunaga, M., Imamoto, N. and Sakata-Sogawa, K. (2008) Highly inclined thin illumination enables clear single-molecule imaging in cells. *Nat Methods* 5: 159-161.
Tran, P.T., Marsh, L., Doye, V., Inoue, S. and Chang, F. (2001) A mechanism for nuclear positioning in fission yeast based on microtubule pushing. *J Cell Biol* 153: 397-411.
Tsai, J.W., Lian, W.N., Kemal, S., Kriegstein, A.R. and Vallee, R.B. (2010) Kinesin 3 and cytoplasmic dynein mediate interkinetic nuclear migration in neural stem cells. *Nat Neurosci* 13: 1463-1471.
Verhey, K.J. and Hammond, J.W. (2009) Traffic control: regulation of kinesin motors. *Nat Rev Mol Cell Biol* 10: 765-777.
Vidali, L., Augustine, R.C., Kleinman, K.P. and Bezanilla, M. (2007) Profilin is essential for tip growth in the moss Physcomitrella patens. *Plant Cell* 19: 3705-3722.
Vidali, L., Rounds, C.M., Hepler, P.K. and Bezanilla, M. (2009) Lifeact-mEGFP reveals a dynamic apical F-actin network in tip growing plant cells. *PLoS One* 4: e5744.
Woehlke, G., Ruby, A.K., Hart, C.L., Ly, B., Hom-Booher, N. and Vale, R.D. (1997) Microtubule interaction site of the kinesin motor. *Cell* 90: 207-216.
Wu, S.Z. and Bezanilla, M. (2014) Myosin VIII associates with microtubule ends and together with actin plays a role in guiding plant cell division. *Elife* 3.
Yang, G., Gao, P., Zhang, H., Huang, S. and Zheng, Z.L. (2007) A mutation in MRH2 kinesin enhances the root hair tip growth defect caused by constitutively activated ROP2 small GTPase in Arabidopsis. *PLoS One* 2: e1074.
Yoo, C.M. and Blancaflor, E.B. (2013) Overlapping and divergent signaling pathways for ARK1 and AGD1 in the control of root hair polarity in Arabidopsis thaliana. *Front Plant Sci* 4: 528.
Yoo, C.M., Wen, J., Motes, C.M., Sparks, J.A. and Blancaflor, E.B. (2008) A class I ADP-ribosylation factor GTPase-activating protein is critical for maintaining directional root hair growth in Arabidopsis. *Plant Physiol* 147: 1659-1674.
Zekert, N. and Fischer, R. (2009) The Aspergillus nidulans kinesin-3 UncA motor moves vesicles along a subpopulation of microtubules. *Mol Biol Cell* 20: 673-684.

Figure legends

Figure 1. The nucleus is translocated to the cell centre in a microtubule (MT)-dependent manner after cell division in apical cells

(**A–C**) Time-lapse imaging (wide-field microscopy) of caulonemal cells expressing GFP-tubulin (green) and HistoneH2B-mRFP (red). The MT-destabilising agent oryzalin (10 μM), actin-destabilising drugs, latrunculin B (25 μM) or cytochalasin B (200 μM), or control (0.5% or 1.0% DMSO) was added to telophase cells at 5-6 min (each group: 2 mL of the solution). Images were acquired every 1 min. Time 0 corresponds to the metaphase-anaphase transition. Dotted lines indicate cell tips at 10 and 90 min. See also Movie 2. Bar, 100 μm. (**D**) The location of the nucleus before and after drug treatment in apical cells. The distance from the metaphase plate (the centre of the chromosome mass at the metaphase) was plotted as mean ± SEM (DMSO, n = 7; oryzalin, n = 7; latrunculin B, n = 6; cytochalasin B, n = 7).

Figure 2. The flowchart of the kinesin RNAi screening

In total, we selected >450 RNAi candidate lines in which 61 genes were targeted with 101 constructs. Time-lapse imaging of the green fluorescent protein (GFP)-tubulin, HistoneH2B-mRFP, and chloroplasts (autofluorescence) was performed using wide-field microscopy. Bars, 10 μm (a metaphase cell), 2 cm (6-well plate), or 100 μm (screened cells).

Figure 3. Kinesins of the ARK subfamily (armadillo repeat-containing kinesins) are necessary for nuclear translocation at the end of cell division

(**A**) Time-lapse imaging (wide-field microscopy) of caulonemal cells expressing GFP-tubulin (green) and HistoneH2B-mRFP (red). The representative control and kinesin-ARK RNAi cells (1st construct, line #7) and the kymographs (**A′**) are displayed. Images were acquired every 3 min. Time 0 corresponds to the start of sister chromatid separation. Horizontal bars, 100 μm; vertical bar, 30 min. See also Movie 4. (**B**) Nuclear movement at the end of cell division in control and kinesin-ARK RNAi apical cells (n = 5 each group, mean ± SEM). The backward movement of the nucleus during 20–40 min in the control cells in this experiment is slightly different from the control cells presented in Fig. 1. We think that this reproducible difference is due to a

difference in culture conditions; in Fig. 1, 0.5 mL of the medium was added to the cells cultured in the agar medium during the course of imaging, whereas in Fig. 3, the cells were examined without addition of the extra medium (however, water was added prior to imaging in order to avoid dryness in the agar). (**C**) The frequency of the nuclear translocation defect after kinesin-ARK RNAi (kinesin-ARK RNAi 1st construct (line #7, n = 25; line #8, n = 15), 2nd construct (line #7, n = 43; line #9, n = 33), 3rd construct (line #2, n = 16; line #3, n = 27), control (n = 75)). For each cell division event, we assessed whether the daughter nucleus in the apical cells moved back to the cell plate.

Figure 4. Abnormal migration of the nucleus in the absence of kinesin-ARK depends on MTs, but not on actin

(**A**–**D**) Time-lapse imaging (wide-field microscopy) of caulonemal cells expressing GFP-tubulin (green) and HistoneH2B-mRFP (red). The actin-destabilising drug latrunculin B (25 μM), or MT-destabilising drug oryzalin (10 μM) was added 20–21 min after the onset of anaphase in the control or kinesin-ARK RNAi cells. Images were acquired every 1 min. Time 0 corresponds to the metaphase-anaphase transition. Bar, 100 μm. See also Movie 5. (**E**) The location of the nucleus before and after drug treatment in the apical cells. The distance from the metaphase plate (the centre of the chromosome mass during the metaphase stage) was measured for multiple RNAi lines. Since the nucleus in all RNAi transgenic lines expressed similar behaviours, we combined the dataset, and plotted the nuclear position as mean ± SEM (control + latrunculin B, n = 5; kinesin-ARK RNAi + latrunculin B, n = 6 (RNAi 2nd construct line #7, n = 3; line #9, n = 2; 3rd construct line #2, n = 1); control + oryzalin, n = 4; kinesin-ARK RNAi + oryzalin, n = 4 (RNAi 2nd construct line #7, n = 1; line #9, n = 3)).

Figure 5. Kinesin-ARK is localised to the MT and around the moving nucleus

(**A**) Time-lapse imaging (spinning-disc confocal microscopy) of caulonemal cells expressing GFP-tubulin (green) and HistoneH2B-mRFP (red). Representative control and kinesin-ARK RNAi cells (2nd construct, line #9) are displayed. Arrowheads indicate MT bundles around the nucleus. Images were acquired every 1 min. See also Movie 6. (**B**) Kinesin ARK-a-Citrine (green) was localised on MTs (red) at the end of cell division. (Left) A cell expressing kinesin ARK-a-Citrine and mCherry-tubulin.

(Right) The parental mCherry-tubulin-expressing cell line. Images were acquired every 1 min. Time 0 corresponds to the start of sister chromatid separation. 'N' indicates the nucleus. See also Movie 7. Bars, 10 μm.

Figure 6. Kinesin-ARK is an MT plus-end-directed motor protein

(**A**) The kinesin-ARK construct used in this *in vitro* experiment. 'CC' indicates the coiled-coil. (**B**) Coomassie staining of purified kinesin-ARK. The protein was further affinity-purified using taxol-stabilised MTs before the assay. (**C**) Quantification of MT gliding velocity in the presence of ATP. Immobile MTs were excluded from the analysis. See also Movie 9. (**D**) Illustration of the MT-gliding assay using a purified motor protein and MTs with marked polarity. Polarity of an MT is indicated by differential fluorescent labelling, in which the fluorescence intensity is higher at the minus end. (**E**) An MT gliding assay using polarity-marked MTs. MTs moved with their minus ends at the front, indicating that kinesin ARK-a is a plus-end-directed motor. Bar, 10 μm.

Figure 7. Nuclear translocation in *P. patens* protonemal apical cell

Schematics of nuclear or spindle positioning in the control and kinesin-ARK RNAi apical cells. After cell division, the daughter nucleus in the apical cells first move towards the cell centre in an MT-dependent manner (phase I). This movement does not require kinesin-ARK or actin. After a while, the nucleus moves backwards, which again depends on MTs, but not on kinesin-ARK or actin (phase II). Before reaching the cell plate, the nucleus moves forward again; this movement depends on MT and kinesin-ARK, but not on actin (phase III). The nucleus is positioned near the cell centre, and this relative position in the cell is maintained for a few hours while the cell tip grows (phase IV). In the absence of kinesin-ARK, the phase III movement is not observed. Instead, the nucleus moves all the way to the cell plate and remains there for a few hours. Before the subsequent mitosis, the nucleus rapidly migrates towards the cell centre. However, the recovery of the position is not complete, and mitosis occurs at a region which is more proximal to the cell plate (phase IV). N.D. stands for 'not determined' in this figure.

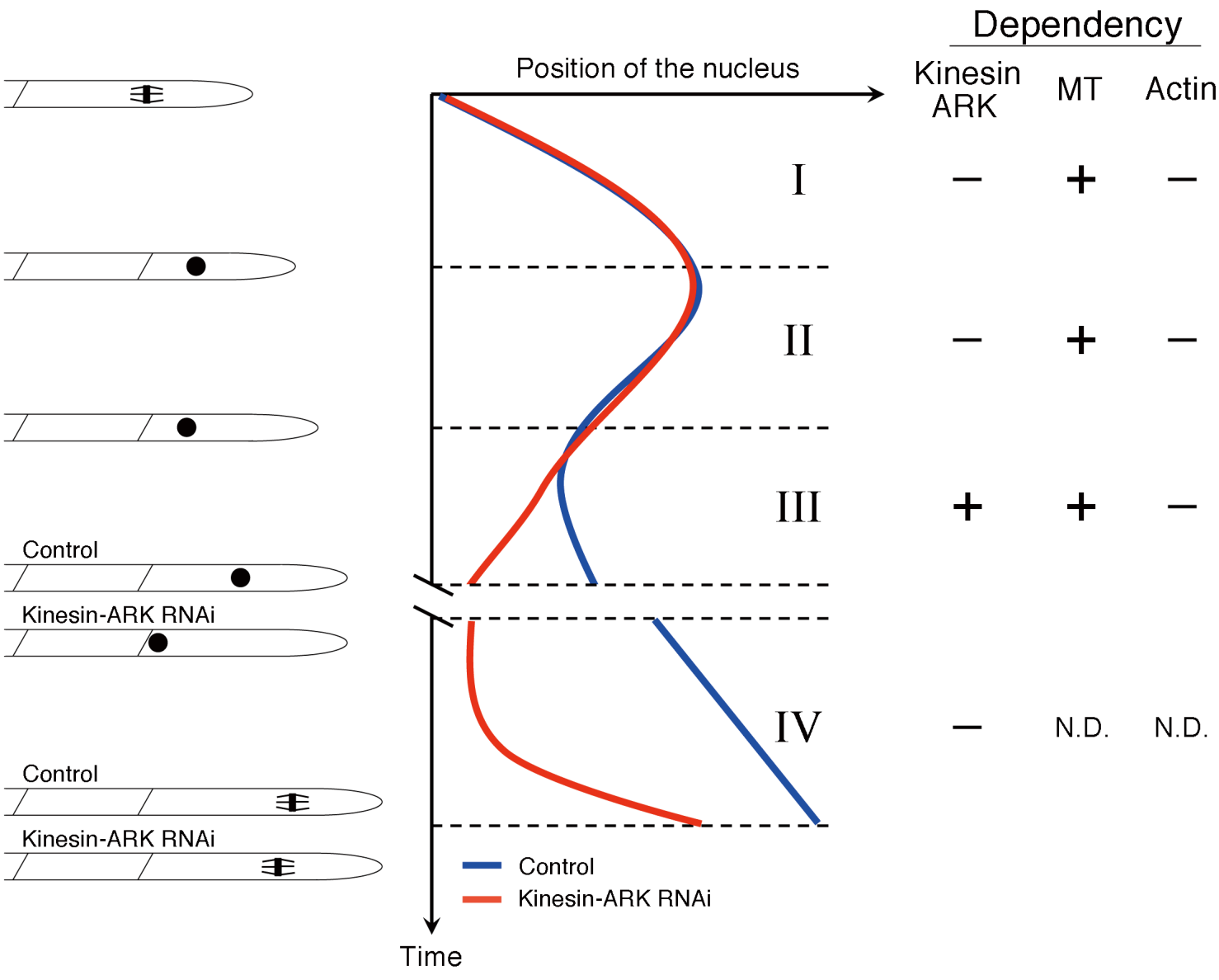
Position of the nucleus
Time
Control
Kinesin-ARK RNAi
Control
Kinesin-ARK RNAi
Control
Kinesin-ARK RNAi
I
II
III
IV
Dependency
Kinesin ARK
MT
Actin
–
+
–
–
+
–
+
+
–
–
N.D.
N.D.

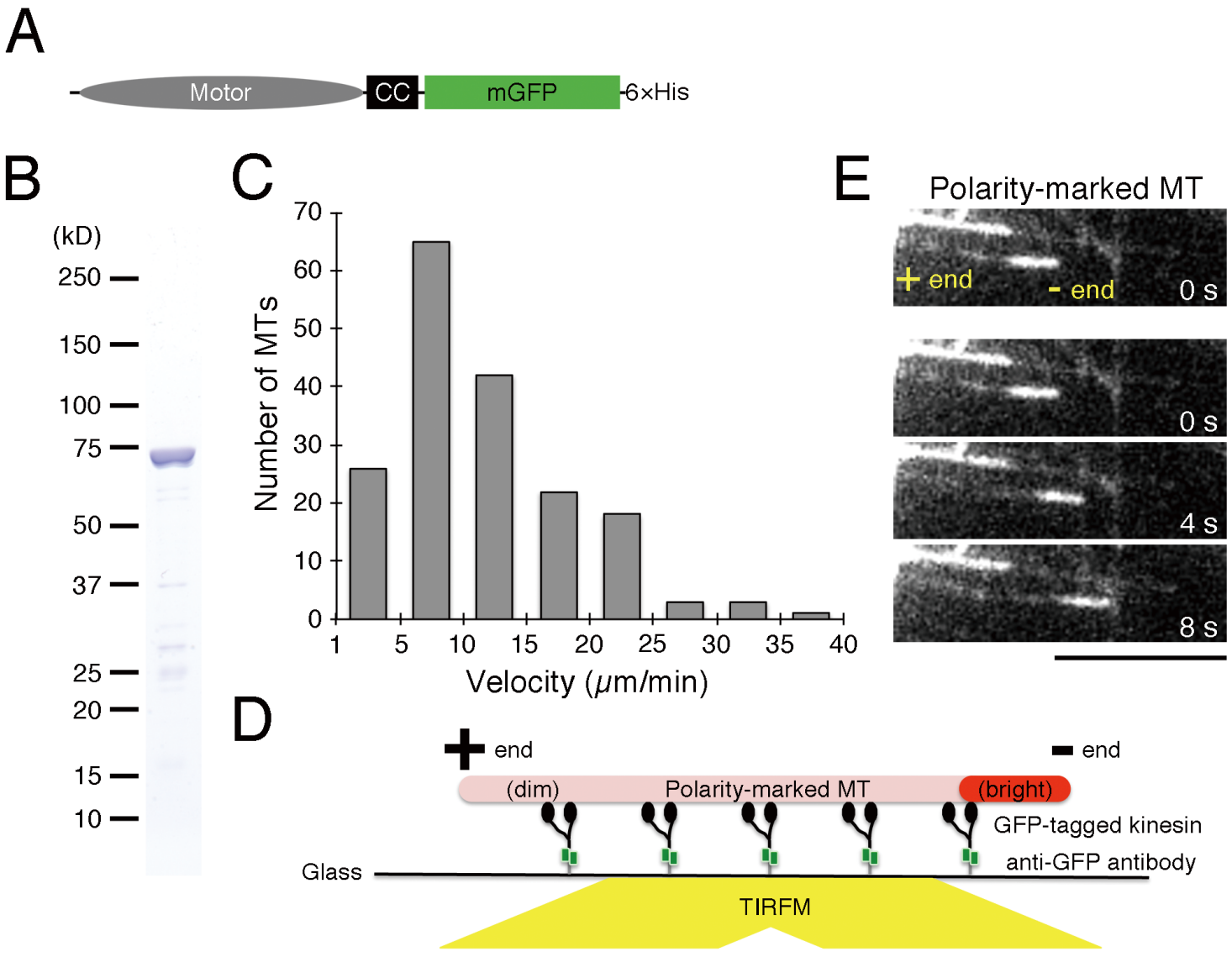
A
Motor
CC
mGFP
6×His
B
(kD)
250
150
100
75
50
37
25
20
15
10
C
Number of MTs
Velocity (μm/min)
D
+ end
- end
(dim)
Polarity-marked MT
(bright)
GFP-tagged kinesin
anti-GFP antibody
Glass
TIRFM
E
Polarity-marked MT
+ end
- end
0 s
0 s
4 s
8 s

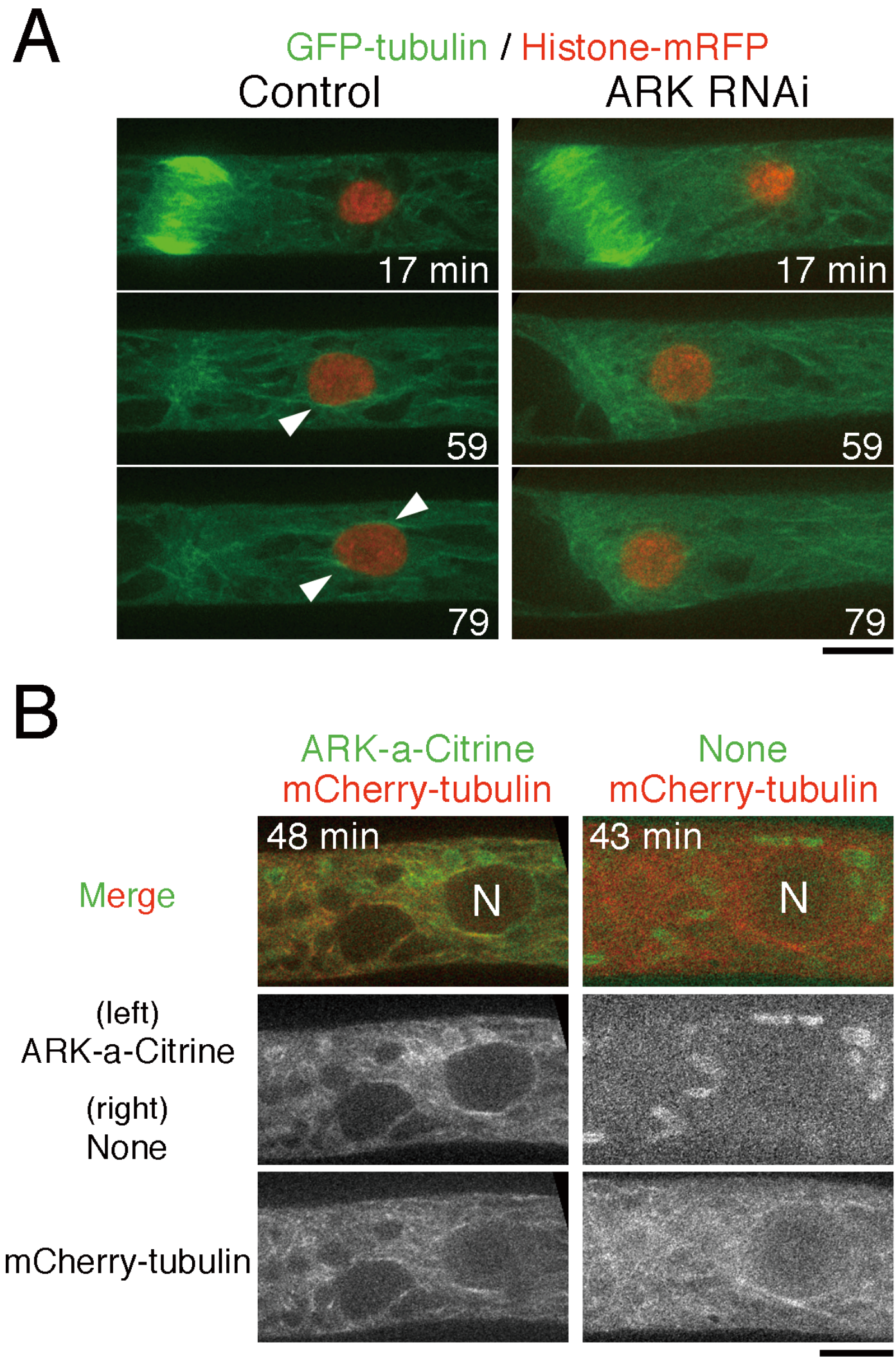
A
GFP-tubulin / Histone-mRFP
Control
ARK RNAi
17 min
17 min
59
59
79
79
B
ARK-a-Citrine
mCherry-tubulin
None
mCherry-tubulin
48 min
N
43 min
N
Merge
(left)
ARK-a-Citrine
(right)
None
mCherry-tubulin

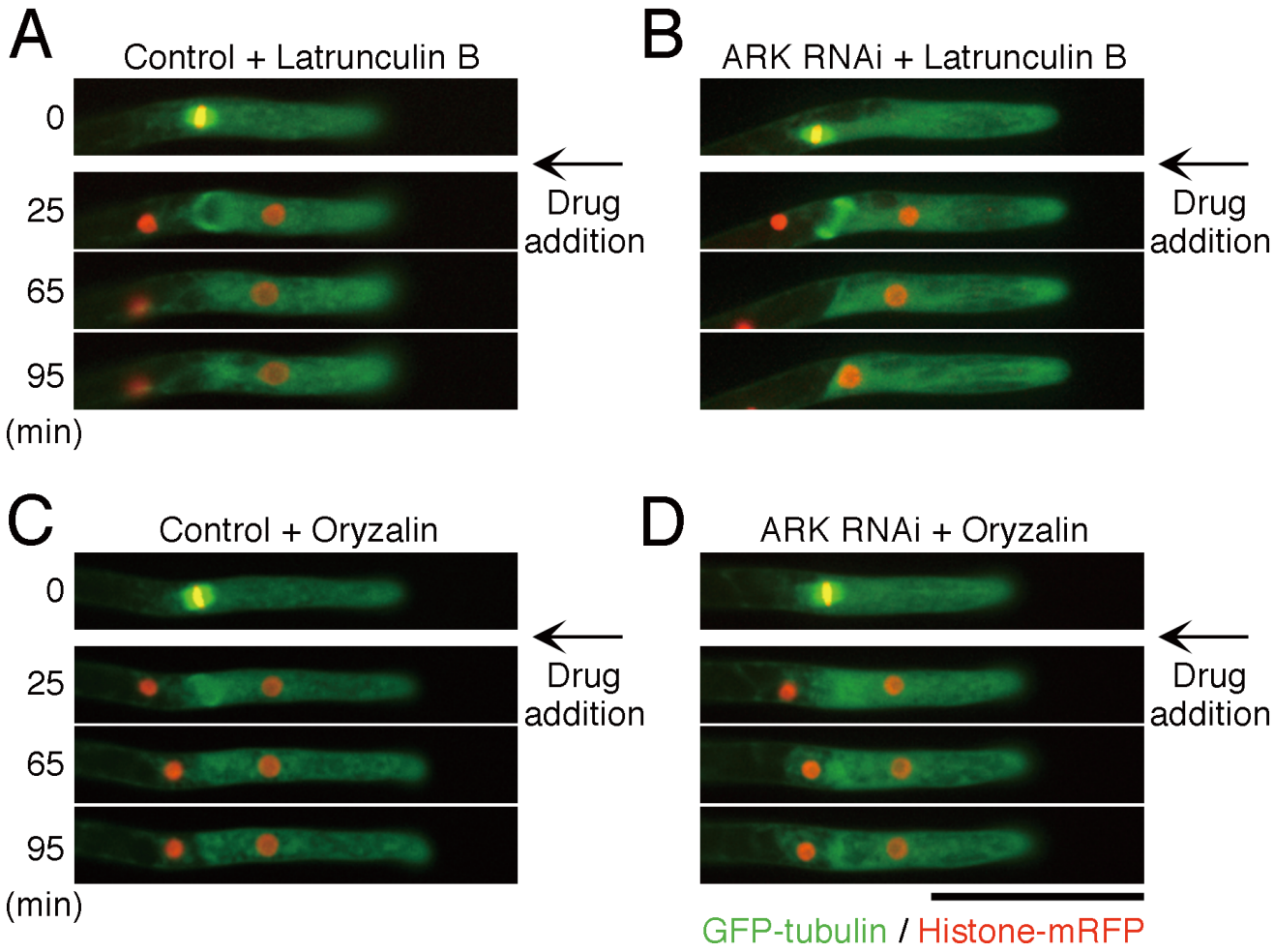
A
Control + Latrunculin B
0
25
65
95
(min)
Drug addition
B
ARK RNAi + Latrunculin B
Drug addition
C
Control + Oryzalin
0
25
65
95
(min)
Drug addition
D
ARK RNAi + Oryzalin
Drug addition
GFP-tubulin / Histone-mRFP

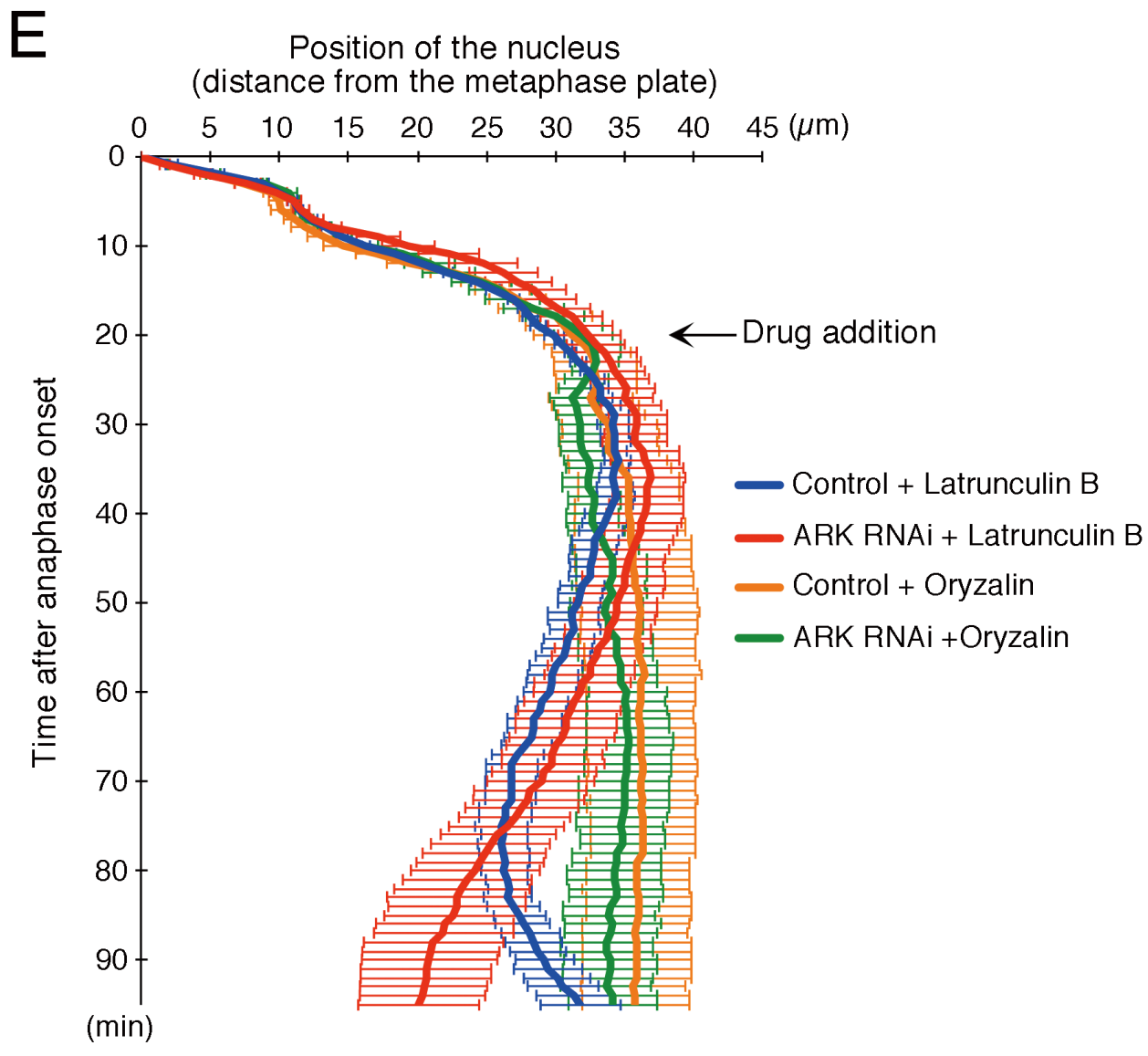
E
Position of the nucleus
(distance from the metaphase plate)
0 5 10 15 20 25 30 35 40 45 (μm)
Time after anaphase onset
0
10
20
30
40
50
60
70
80
90
(min)
Drug addition
Control + Latrunculin B
ARK RNAi + Latrunculin B
Control + Oryzalin
ARK RNAi +Oryzalin

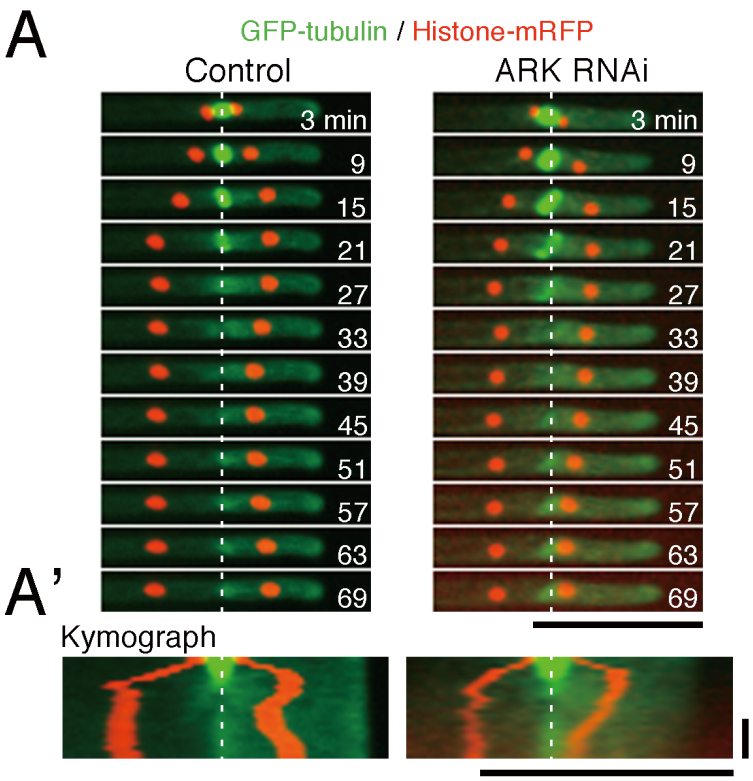
A
GFP-tubulin / Histone-mRFP
Control
ARK RNAi
3 min
9
15
21
27
33
39
45
51
57
63
69
A'
Kymograph

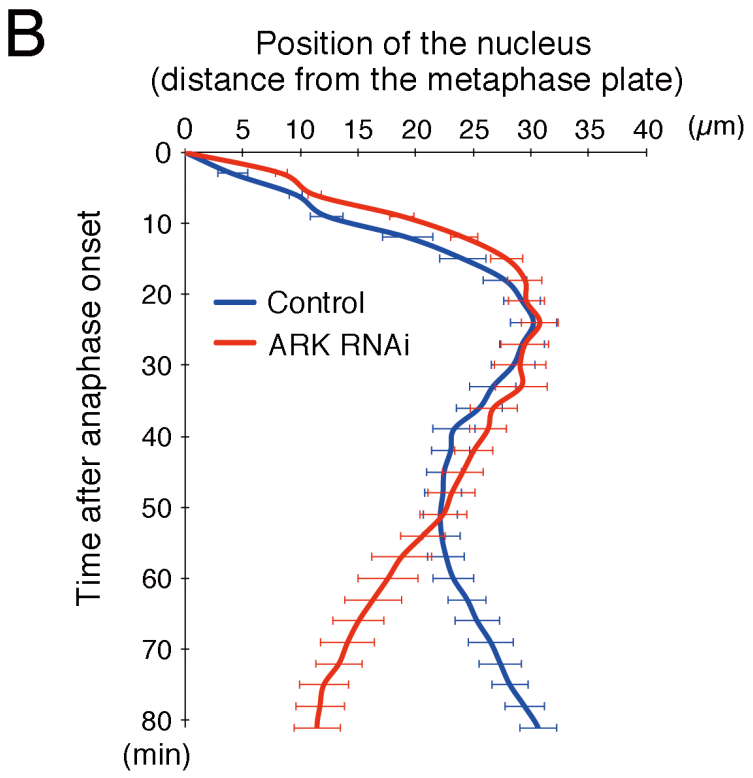
B
Position of the nucleus
(distance from the metaphase plate)
0 5 10 15 20 25 30 35 40 (μm)
Time after anaphase onset
0
10
20
30
40
50
60
70
80
(min)
Control
ARK RNAi

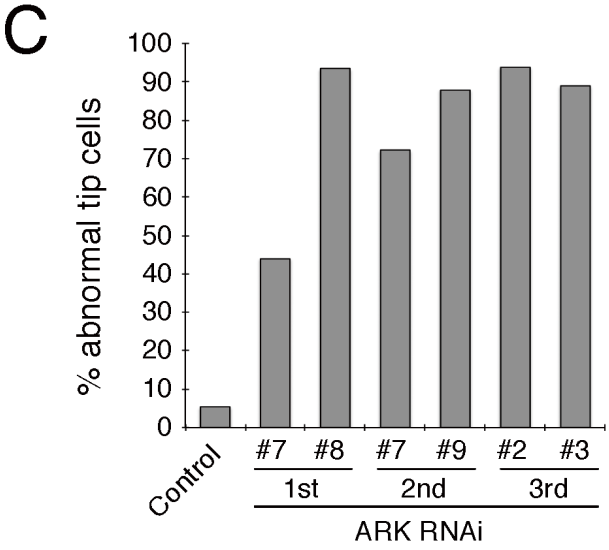
C
% abnormal tip cells
100
90
80
70
60
50
40
30
20
10
0
Control
#7
#8
#7
#9
#2
#3
1st
2nd
3rd
ARK RNAi

• 78 kinesins in *Physcomitrella patens*

BLAST search

• Designing 2 sets of PCR primers against 78 kinesins
• PCR amplification (~700 bp)

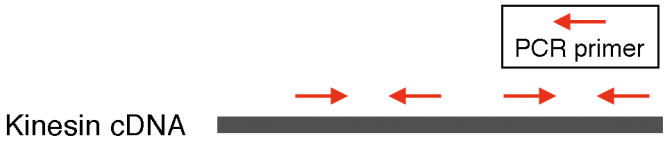

• Insertion to pENTR/D-TOPO vector
• Gateway LR reaction to the pGG626 RNAi vector

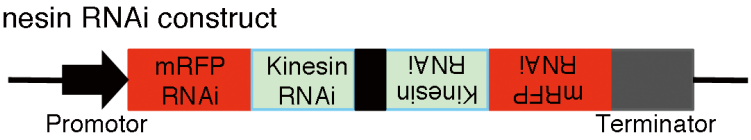

• Transformation of RNAi constructs to the GFP-tubulin/Histone-mRFP cell line

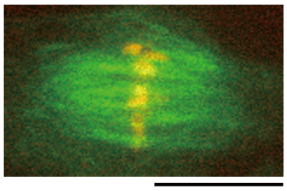

GFP-tubulin
Histone-mRFP

• Histone-mRFP intensity screening
• Imaging (long-term, multiple positions)

6-well glass-bottom dish

• Manual inspection of the phenotypes

Total
61 genes
101 constructs
> 450 lines observed

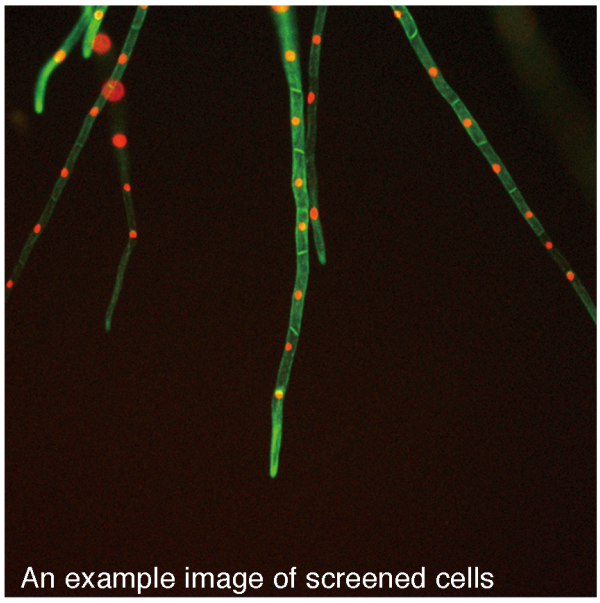

An example image of screened cells

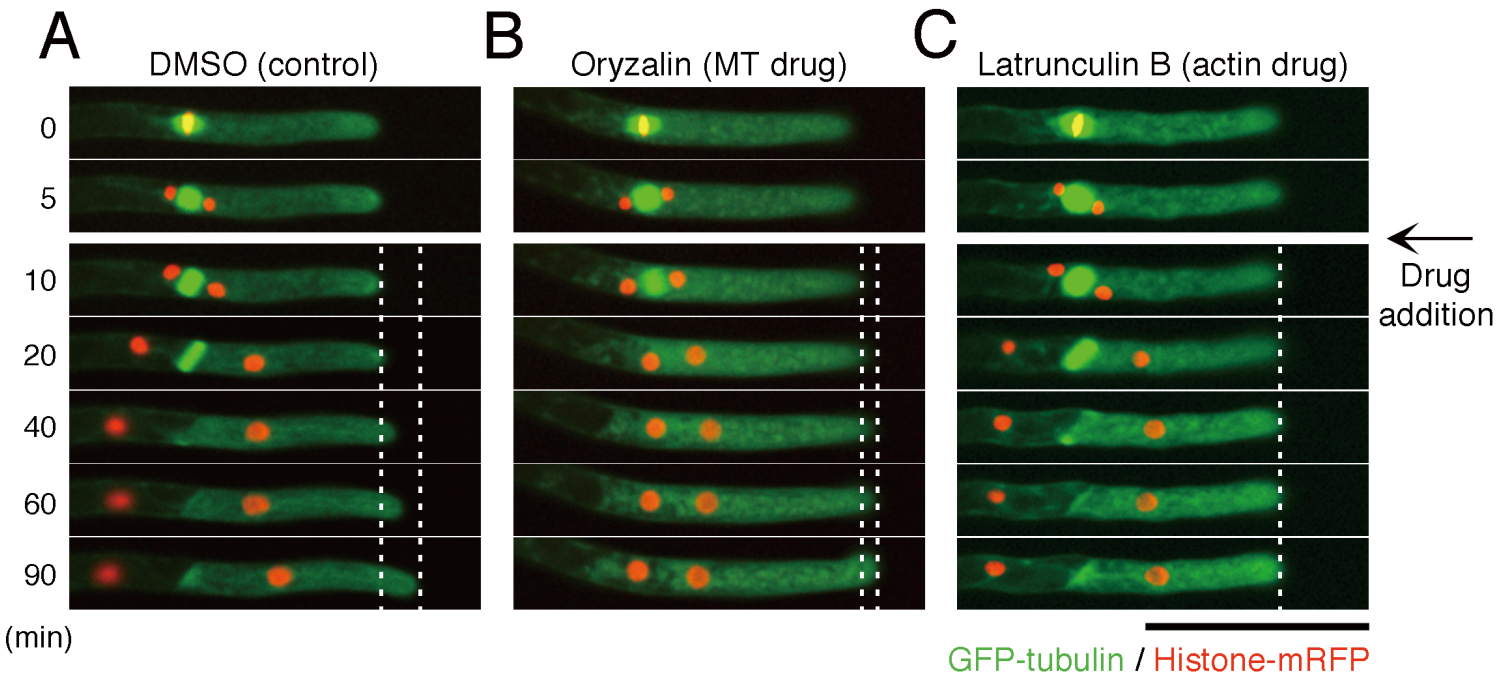
A
DMSO (control)
B
Oryzalin (MT drug)
C
Latrunculin B (actin drug)
0
5
10
20
40
60
90
(min)
Drug addition
GFP-tubulin / Histone-mRFP

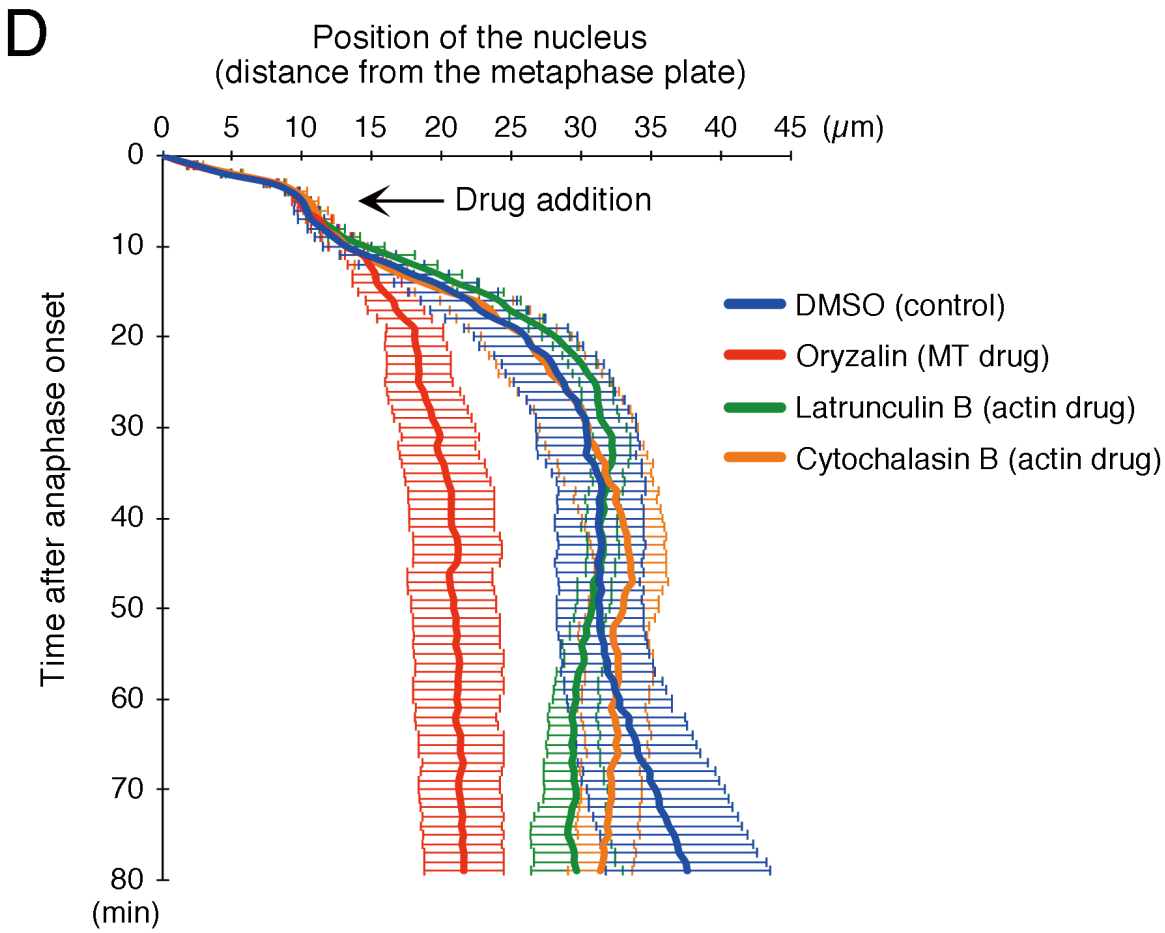
D
Position of the nucleus
(distance from the metaphase plate)
0 5 10 15 20 25 30 35 40 45 (μm)
Drug addition
Time after anaphase onset
0
10
20
30
40
50
60
70
80
(min)
DMSO (control)
Oryzalin (MT drug)
Latrunculin B (actin drug)
Cytochalasin B (actin drug)